THE JOURNAL OF PHYSICAL CHEMISTRY B

Article

pubs.acs.org/JPCB

Molecular Mechanism of the Inhibition of EGCG on the Alzheimer $A\beta_{1-42}$ Dimer

Tong Zhang,[†,§] Jian Zhang,[‡] Philippe Derreumaux,[§,¶] and Yuguang Mu*[,†]

[†]School of Biological Sciences, Nanyang Technological University, 60 Nanyang Drive, Singapore 637551

[‡]Department of Physics, National Laboratory of Solid State Microstructure and Department of Physics, Nanjing University, Nanjing, Jiangsu 210093, China

[§]Laboratoire de Biochimie Théorique, Institut de Biologie Physico-Chimique, UPR9080, CNRS, Université Denis Diderot, Sorbonne Paris Cité, 13 rue Pierre et Marie Curie, 75005 Paris, France

[¶]Institut Universitaire de France, 103 Bvd Saint-Michel, 75005 Paris, France

Supporting Information

ABSTRACT: Growing evidence supports that amyloid β (Aβ) oligomers are the major causative agents leading to neural cell death in Alzheimer's disease. The polyphenol (−)-epigallocatechin gallate (EGCG) was recently reported to inhibit Aβ fibrillization and redirect Aβ aggregation into unstructured, off-pathway oligomers. Given the experimental challenge to characterize the structures of Aβ/EGCG complexes, we performed extensive atomistic replica exchange molecular dynamics simulations of $A\beta_{1-42}$ dimer in the present and absence of EGCG in explicit solvent. Our equilibrium Aβ dimeric structures free of EGCG are consistent with the collision cross section from ion-mobility mass spectrometry and the secondary structure composition from circular dichroism experiment. In the presence of EGCG, the Aβ structures are characterized by increased inter-center-of-mass distances, reduced interchain and intrachain contacts, reduced β-sheet content, and increased coil and α-helix contents. Analysis of the free energy surfaces reveals that the Aβ dimer with EGCG adopts new conformations, affecting therefore its propensity to adopt fibril-prone states. Overall, this study provides, for the first time, insights on the equilibrium structures of $A\beta_{1-42}$ dimer in explicit aqueous solution and an atomic picture of the EGCG-mediated conformational change on Aβ dimer.

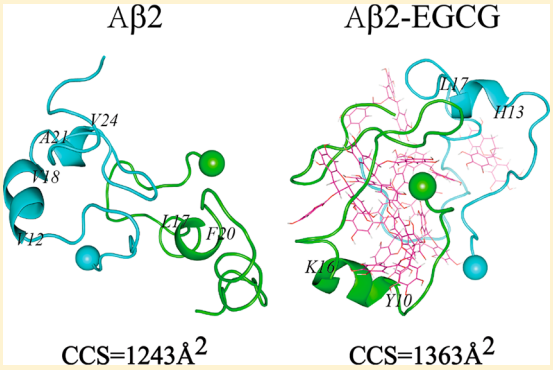

1. INTRODUCTION

Many human neurodegenerative diseases including Parkinson, Huntington, Creutzfeldt−Jakob, and Alzheimer's are associated with the formation of amyloid plaques.[1−4] These insoluble deposits with cross-β structure result from the self-assembly of proteins with diverse sequences, structures, and functions. In Alzheimer's disease (AD), the plaques found in brain tissues consist mainly of the amyloid β (Aβ) proteins of 36−43 amino acids, produced from the cleavage of the amyloid precursor protein.[5,6] There is strong evidence, however, that the low molecular weight oligomers are the most neurotoxic agents.[7,8]

Characterizing the Aβ dimer, the smallest oligomer, at atomic level is therefore critical for understanding or inhibiting Aβ fibrillization. Because Aβ has a very high propensity to associate/dissociate and is metastable, we only have low-resolution experimental data on the dimers. Using ion-mobility mass spectrometry, Bernstein et al. reported a collision cross section of 1256 Å^2 for $A\beta_{1-42}$ dimer.[9] Using different preparation methods and CD analysis, Teplow et al. reported a β-strand content varying between 12% and 25% and an α-helix content varying from 3% to 9% at 295 K, pH 7.5, and day 0, for therefore a mixture of various aggregates.[10,11] Given the experimental challenge to characterize the structures, several computer simulations have been conducted on $A\beta_{1-42}$ dimer. However, most of them used either coarse-grained models[12,13] or an atomistic protein model with an implicit solvent representation.[14] Recently, Chong and Ham performed one all-atom MD simulation of 100 ns in explicit solvent and investigated the early steps of dimerization.[15] Zhu et al. carried out 10 MD runs, each of 80 ns, starting from different configurations.[16] Barz and Urbanc performed all-atom MD trajectories of 50 ns using two explicit solvent models starting from 42 structures generated by coarse-grained discontinuous (DMD) simulations.[17] Though these studies provided structural information, multiple MD simulations of 50−80 ns cannot converge to the conformational equilibrium ensemble, and therefore convincing structures for $A\beta_{1-42}$ dimer are still missing.

Received: December 20, 2012
Revised: March 15, 2013
Published: March 28, 2013

   dx.doi.org/10.1021/jp312573y | J. Phys. Chem. B 2013, 117, 3993−4002

Another important issue is the design of efficient antiamyloid agents. Many small molecules have been identified to inhibit amyloid formation, such as curcumin,[18] 2002-H20,[19] Nqtrp,[20] resveratrol,[21] and EGCG.[22,23] Among others, EGCG, a polyphenol compound extracted from green tea, has been reported to produce unstructured, off-pathway oligomers and reduce toxicity of α-synuclein and Aβ_{1-42} peptides.[22,23] Thermodynamic analysis of the molecular interactions between the Aβ_{1-42}, Aβ_{1-16}, Aβ_{1-30}, and Aβ_{1-42} peptides and EGCG at different EGCG and salt concentrations was also conducted by isothermal titration calorimetry. The results revealed that the interactions between Aβ_{1-42} and EGCG are mainly hydrogen bonding in the region 1−16 and hydrophobic in the region 17−42.[24,25] All-atom MD simulations of the Aβ_{1-42} monomer at different EGCG concentrations (0, 5, and 10 EGCG molecules) were also performed for 300 ns at 300 and 330 K using the GROMOS force field and the single point charge (SPC) model.[26] Starting from an Aβ_{1-42} conformation with 71% of α-helix, the MD simulation free of any EGCG molecule still averaged 40% of α-helix within 200−300 ns, versus 3−9% from CD,[10,11] indicating thereby limited sampling of the energy landscape. In addition, it is well-known that the monomer and the dimer have distinct structural features.[11,13,27,28]

In this study, to overcome insufficient MD sampling, we performed extensive atomistic replica exchange molecular dynamics (REMD) simulations of Aβ_{1-42} dimer in explicit solvent with and without the presence of EGCG molecules. While several numerical studies investigated the interactions of inhibitors with preformed protofibrils or oligomers of Aβ fragments using all-atom MD in explicit[29−31] and implicit solvents,[32] or coarse-grained model,[33] REMD simulations in explicit solvent have not been performed thus far. Our aim is to characterize the structures that Aβ_{1-42} dimer adopts in both the absence and presence of EGCG, thereby providing a full picture of the EGCG-mediated conformational change on Aβ_{1-42} dimer.

2. METHODS

2.1. Simulation Details. The Aβ_{1-42} sequence is DAEFRHDSGY[10] EVHHQKLVFF[20] AEDVGSNKGA[30] IIGLMVGGVV[40] IA. The initial coordinates of Aβ_{1-42} monomer were taken from model 1 of the PDB entry 1IYT.[34] This conformation observed by NMR in an apolar environment is characterized by two α-helices spanning residues 8−25 and 28−39 (Figure 1A). The monomer with the N- and C-terminals treated as NH_3^+ and COO^- was then replicated and translated so that the initial dimer with parallel orientation of the peptides did not display any interchain atomic distances <10 Å. The OPLS-AA force field[35] was used rather than the GROMOS or older versions of AMBER force fields because the OPLS-generated conformations for the Aβ_{1-40} and Aβ_{1-42} monomer best match the NMR data.[36] In addition, many studies have shown that OPLS is suitable for exploring the aggregation of several Aβ fragments in explicit water,[37] and gives results qualitatively similar to that found using CHARMM force field for the Aβ_{10-35} dimer.[38] EGCG taken from the PubChem Compound library (Figure 1B) was first energy minimized using Spartan'10[39] and then further optimized at the HF/6-31G* level using Gaussian09 software.[40] The atomic partial charges were derived using the R.E.D III package.[41] Other EGCG parameters were assigned based on the OPLS-AA force field.

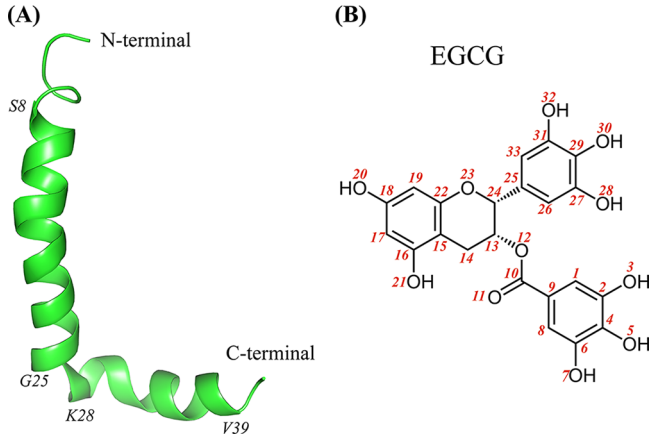

Figure 1. Structures of Aβ monomer and EGCG molecule. (A) The initial Aβ conformation. The main chain of the peptide is shown by cartoon model using Pymol. (B) The chemical structure of EGCG molecule. The red and italic numbers label the heavy atoms.

In both simulations, Aβ dimer was initially put in the center of a dodecahedron box with periodic boundary conditions, with a distance of 7 Å between the protein surface and box boundary. The initial volume of the box is ~285 nm^3. For the Aβ2−EGCG system, 10 EGCG molecules were randomly added into the simulation box. This molar ratio of EGCG to Aβ matches that used experimentally by Ehrnhoefer et al.[22] Then, 8752 and 8537 SPC water molecules[42] were added into the boxes for Aβ2 and Aβ2−EGCG, respectively. Finally, 6 Na^+ ions were added by randomly replacing water molecules to make the systems neutral. Recently, it has been shown that the SPC, TIP3P, and SPC/E water models have similar performance in most energetic and structural properties in a MD simulation of a protein in crystal, although SPC/E outperforms in water diffusion; and the dynamics of the protein was well preserved.[43] This indicates that the results on our systems should not vary much using SPC/E water model.

The GROMACS program (version: 4.5.4)[44] was used to perform the simulations. The LINCS protocol[45] was used to constrain the bonds involving hydrogen atoms, allowing an integration time step of 2 fs. The particle mesh Ewald method[46] with a cutoff of 0.9 nm was used to treat the electrostatic interactions. A cutoff of 1.2 nm was used for the van der Waals interactions. The nonbonded pair lists were updated every 0.010 ps. The coordinates were saved every 1 ps. REMD simulations[47,48] were carried out with 64 replicas with temperature ranging from 315 to 450 K by the method described by Patriksson and van der Spoel.[49] Temperatures were controlled by the Bussi−Donadio−Parrinello velocity rescaling thermostat found to sample the canonical ensemble.[50] Exchanges between neighboring replicas were attempted every 2 ps, leading to an acceptance ratio of 33% and 34% in both simulations. Each REMD simulation ran for 200 ns.

2.2. Simulation Analysis. The time-averaged normalized ratio of water oxygen atoms, g_{NOW}, was used to reflect the distribution of EGCG molecules around Aβ. Following Lerbret et al.[51] and Liu et al.,[26] g_{NOW} is computed by

$$g_{NOW}(r) = \frac{n_{OW}(r)/[n_{OW}(r) + n_{OE}(r)]}{N_{OW}/(N_{OW} + N_{OE})} \quad (1)$$

where $n_{OW}(r)$ and $n_{OE}(r)$ are the number of water oxygen atoms and hydroxyl oxygen atoms of EGCG at the distance, r,

dx.doi.org/10.1021/jp312573y | J. Phys. Chem. B 2013, 117, 3993−4002

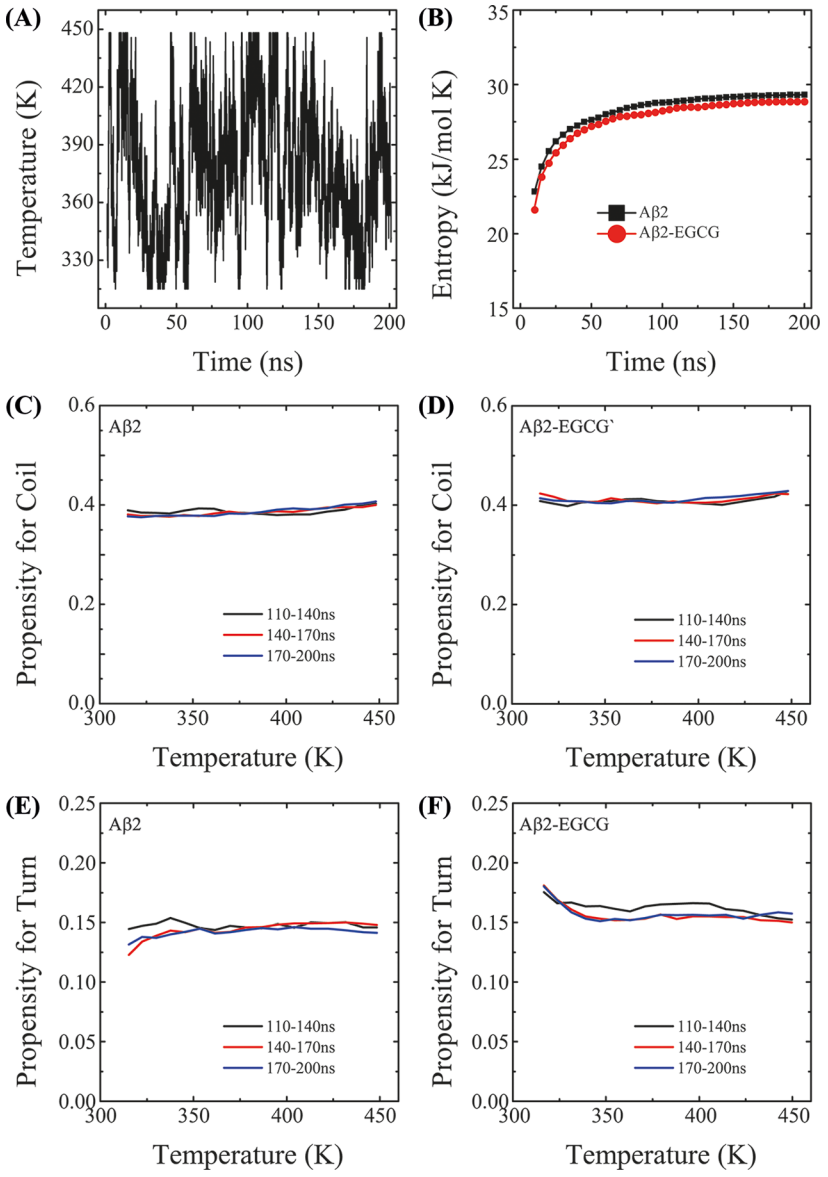

Figure 2. Simulation convergence assessments. (A) Evolution of one selected replica in temperature space as a function of time for Aβ2. (B) Time evolution of entropy as estimated by the quasiharmonic approach. (C) Propensity for coil in the Aβ2 system as a function of temperature in the time intervals 110−140, 140−170, and 170−200 ns. (D) Propensity for coil in the Aβ2−EGCG system as a function of temperature in the time intervals 110−140, 140−170, and 170−200 ns. (E) Propensity for turn in the Aβ2 system as a function of temperature in the time intervals 110−140, 140−170, and 170−200 ns. (F) Propensity for turn in the Aβ2−EGCG system as a function of temperature in the time intervals 110−140, 140−170, and 170−200 ns.

from the protein surface, respectively. N_{OW} and N_{OE} are the total number of water oxygen and hydroxyl oxygen atoms of EGCG, respectively. To monitor the dimerization of Aβ, the interchain center-of-mass distance, dCM, was determined using the command g_dist in GROMACS, with the center-of-mass based on the heavy atoms only. The number of interchain contacts between either the two Aβ peptides, or between Aβ and EGCG, and the number of contacts within each peptide were defined as the numbers of heavy atom pairs with a distance <5 Å. A salt bridge was considered formed when the distance between the side chain nitrogen atoms of a positively charged residue and the side-chain oxygen atoms of negatively charged residues was <3.2 Å. A hydrogen bond was considered formed when the acceptor−donor distance was not more than 3.5 Å; meanwhile the acceptor−donor−hydrogen angle was not more than 30°.

The secondary structures of Aβ were calculated using the DSSP algorithm.[52] The dihedral principal component analysis was used to construct the free energy landscape following the protocol described by Mu et al.[53] The backbone dihedral angles from both simulations were calculated and concatenated to construct a covariance matrix and find the eigenvectors common in both systems. Then, the two trajectories were projected separately onto the first two common eigenvectors, dPC1 and dPC2. By using this procedure, it is meaningful to directly compare the configuration spaces based on the free energy landscapes. For each dominant local minimum, we performed a clustering analysis based on pairwise rmsd structural comparison. The collision cross section (CCS) of the dimeric structures was calculated using the MOBCAL software[54,55] and the trajectory method[55] which treats the target molecule as a collection of atoms represented by a 12−

dx.doi.org/10.1021/jp312573y | J. Phys. Chem. B 2013, 117, 3993−4002

6−4 potential. This method, often used for proteins,[15] has been shown to have an accuracy of 99% for ondansetron and its hydroxylated metabolites.[56] Finally, the conformational entropy was calculated using the quasiharmonic approximation.[57]

2.3. Binding Free Energy Calculations. The binding free energy was calculated based on the MM/PBSA method[58] using AMBER program suite version 10.[59] For both systems, 1000 snapshots were extracted from 100 to 200 ns with a time interval of 100 ps. The binding free energy for Aβ dimer was estimated by

$$\Delta G_{\text{binding}} = G_{\text{dimer}} - (G_{\text{monoA}} + G_{\text{monoB}}) \quad (2)$$

The binding free energy for Aβ dimer−EGCG complex was estimated by

$$\Delta G_{\text{binding}} = G_{\text{complex}} - (G_{\text{monoA}} + G_{\text{monoB}} + G_{\text{EGCG}}) \quad (3)$$

where each energy term, G, is estimated as the sum of the gas-phase molecular mechanics energy E_{gas}, and the solvation energy G_{sol} according to eq 4

$$G_{\text{total}} = E_{\text{gas}} + G_{\text{sol}} \quad (4)$$

with E_{gas} containing an electrostatic term (E_{ele}) and a van der Waals term (E_{vdw}) including the 1−4 interactions. Notably, the contribution of entropy was neglected in the binding free energy reported here.[60] The solvation energy is further decomposed into the polar solvation energy G_{ps} and the nonpolar solvation energy G_{nps}:

$$G_{\text{sol}} = G_{\text{ps}} + G_{\text{nps}} \quad (5)$$

The polar solvation energy G_{ps} was calculated by solving the Poisson−Boltzmann equation using the MM/PBSA module, with the dielectric constants set to 1 for solute and 80 for solvent, and the ionic strength set to 0 as reported in ref 26. The nonpolar solvation energy was estimated based on the solvent-accessible surface area (SASA), according to $G_{\text{nps}} = \gamma \times \text{SASA} + \beta$. The surface tension coefficient γ and constant β were set to 0.005 42 kcal/(mol·Å^2) and 0.92 kcal/mol, commonly used in the literature.[26,61,62] The water probe radius to calculate the SASA was 1.4 Å.

2.4. Terminology. The Aβ peptide was segmented into four regions: the N-terminal (residues 1−16), the central hydrophobic core (CHC) (residues 17−21), the fibril-loop region (residues 22−28), and the C-terminal (residues 29−42). For simplicity, in what follows, Aβ2 and Aβ2−EGCG refer to the simulation of Aβ_{1-42} dimer in the absence and presence of EGCG, respectively.

3. RESULTS

3.1. Convergence Assessment. The simulation efficiency was monitored by several criteria. As shown in Figure 2A, one representative replica visits a wide range of temperatures during 200 ns. Other replicas show similar behavior (data not shown), indicating an efficient walk in temperature space. The conformational entropy at the lowest temperature, 315 K, shown in Figure 2B, remains constant after 100 ns. Note that the entropy in Aβ2−EGCG is slightly lower than that of Aβ2, suggesting different global Aβ dynamics in both systems. The coil and turn contents of the peptides as a function of temperature are shown in both systems using three different time intervals, 110−140, 140−170, and 170−200 ns (Figure 2C−F). We see that the propensities for coil and turn have converged in both systems. Figure 3A shows the time evolution

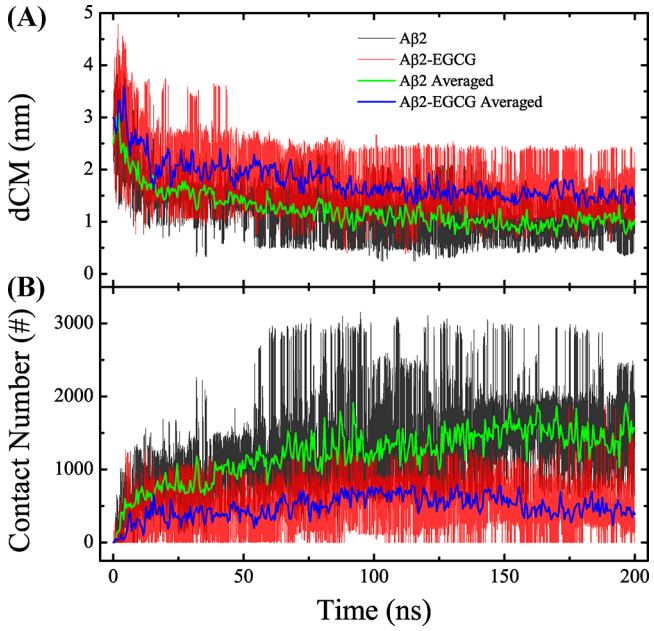

Figure 3. Time evolution of two global properties of Aβ dimers. To clarify, the averaged values on every 500 ps are also shown. (A) The inter-center-of-mass distance, dCM, between the two Aβ peptides in the Aβ2 (black solid line) and Aβ2−EGCG (red solid line) systems. The averaged values of dCM between Aβ peptides in the Aβ2 (green solid line) and Aβ2−EGCG (blue solid line) systems. (B) The total number of heavy atom contacts between the two Aβ peptides in the Aβ2 (black solid line) and Aβ2−EGCG (red solid line) systems. The averaged total number of heavy atom contacts between the two Aβ peptides in Aβ2 (green solid line) and Aβ2−EGCG (blue solid line) systems.

of the inter-center-of-mass distance, dCM, between the two Aβ peptides at 315 K. In both systems, the Aβ peptides approached gradually in the first 100 ns, and then dCM remains constant within 100−200 ns at 1.2 nm in Aβ2 and 1.6 nm in Aβ2−EGCG. Figure 3B shows the time evolution of the total number of heavy atom contacts between the two Aβ peptides in Aβ2 and Aβ2−EGCG at 315 K. The number of contacts increases substantially during the first 100 ns, and then fluctuates around an averaged value of 1440 in Aβ2 and 540 in Aβ2−EGCG within 100−200 ns. Finally, Figure 4 shows the coil propensity of each amino acid along the sequence in both systems at 315 K using the time intervals 110−140, 110−170, and 110−200 ns. We see that the percentage of coil remains fully constant as the simulation progresses from 100 to 200 ns. Taken together, all these results provide strong evidence that the conformational ensemble has reasonably converged within 200 ns. In what follows the analysis is based on the configuration ensemble at 315 K using 100−200 ns and the statistical errors are based on the interval of confidence on the mean value by Boostrap analysis.

3.2. EGCG Molecules Directly Bind to Aβ Peptides. The binding of EGCG to Aβ was first examined by the time-averaged normalized ratio of water oxygen atoms, g_{NOW}, as a function of distance from the closest Aβ atom (Figure 5). The EGCG molecules strongly interact with Aβ peptides as seen from the g_{NOW} values <1 for all distances <1.4 nm and the presence of a minimum at 0.3 nm. This distribution is consistent with all-atom MD simulations studying the interaction of Aβ_{1-42} monomer with 10 EGCG molecules, albeit the two profiles do not superpose on each other.[26] The

dx.doi.org/10.1021/jp312573y | J. Phys. Chem. B 2013, 117, 3993−4002

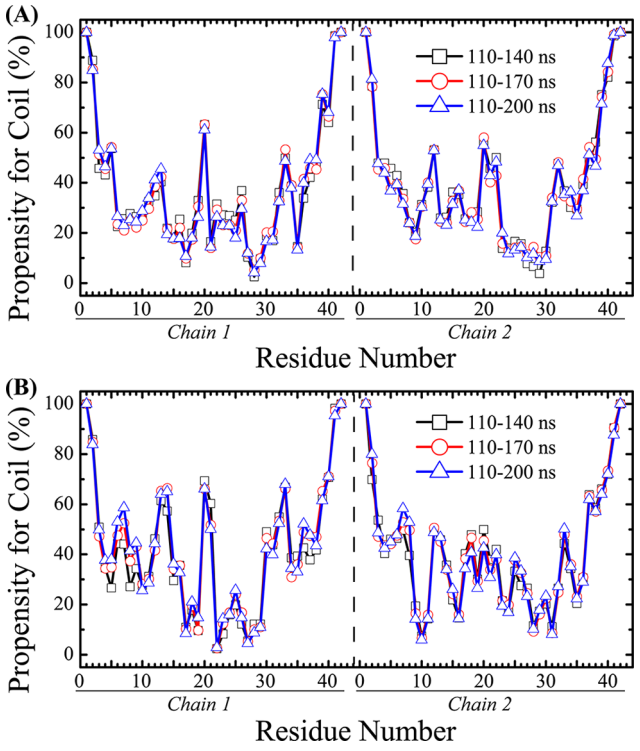

Figure 4. Coil propensity as a function of each Aβ amino acid in both systems at 315 K using three time windows, 110−140, 110−170, and 110−200 ns: (A) Aβ2 system; (B) Aβ2−EGCG system.

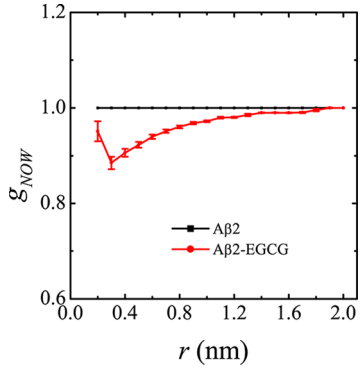

Figure 5. Time-averaged normalized ratio of water oxygen atoms, g_{NOW}, as a function of distance from the closest Aβ_{1-42} atom. The black line with squares is for Aβ2 system, while the red line with circles is for the Aβ2−EGCG system. Error bars are shown.

binding of EGCG to Aβ peptides was further evaluated by the contact maps between the heavy atoms of EGCG and Aβ. Panels A and B in Figure 6 show the results for the main-chain atoms and the side-chain atoms of Aβ, respectively. The three outward aromatic rings display a higher number of contacts with Aβ peptides than the carboxyl groups and the heterocyclic ring. While the EGCG molecules interact preferentially with the main-chain atoms of residues Gly29/Ala30, Gly37/Gly38/Val39, Ala42, and then Arg5, they strongly interact with the side-chains of residues Phe4, Phe19/Phe20, Tyr10, Ile31/Ile32, Met35/Val36, Val39, and Ile41. These results, along with the small solvent accessible surface areas of EGCG molecules (Supporting Information, Figure S1) and the occupancy of hydrogen bonds between Aβ and EGCG (Supporting Information, Figure S2), indicate that EGCG are buried in

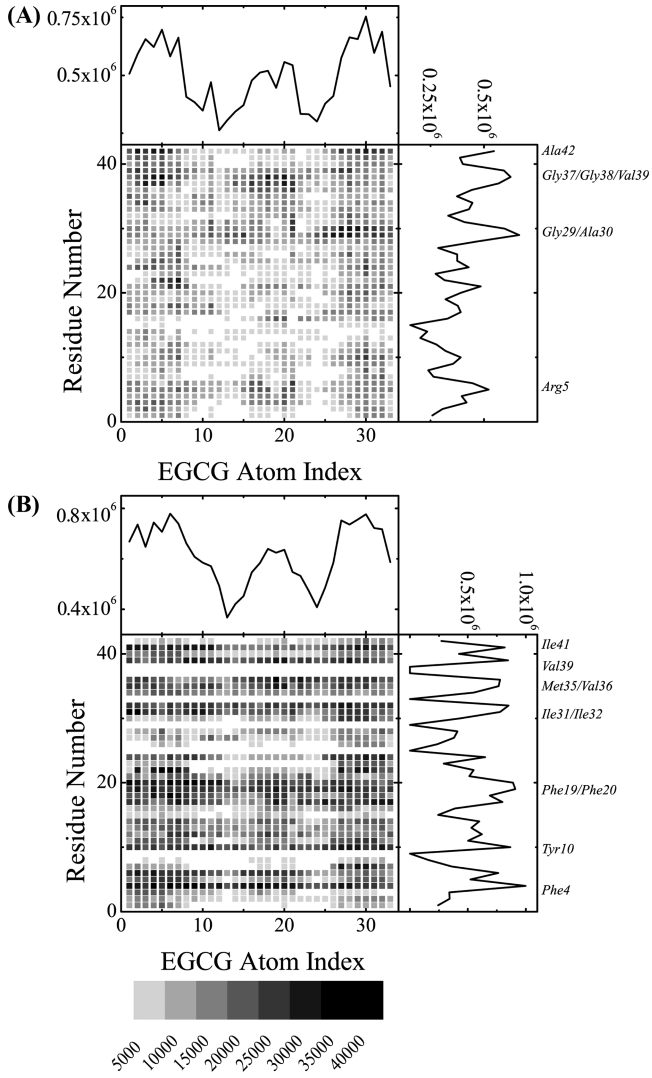

Figure 6. Contact maps between the heavy atoms of EGCG and the Aβ_{1-42} amino acids. (A) Interactions with the backbone Aβ atoms. (B) Interactions with the side-chain Aβ atoms. The labeling of the heavy EGCG atoms is shown in Figure 1B. The color scale reflects the numbers of contacts. The cumulative numbers of contacts for each heavy atom of EGCG and Aβ are shown in the upper and right panels, respectively. Amino acids with high number of contacts are labeled.

the interface between the Aβ peptides and bind mostly to the hydrophobic residues of the CHC and C-terminal region through van der Waals interactions, and mostly to the N-terminal amino acids Asp1, Glu3, Arg5, Asp7, and Glu11 through H-bonds, albeit H-bonds with residues Ala21/Glu22/Asp23 and Ile32 are also present. Overall, our pattern of interactions between EGCG and Aβ_{1-42} is fully consistent with that derived from isothermal titration calorimetry experiments.[24,25]

3.3. Effects of EGCG on the 2D and 3D Structures of Aβ Dimer. Table 1 gives the secondary structure compositions in both systems. Notably, the percentages do not change much. In (Aβ2 and Aβ2−EGCG) systems, coil is the most populated (36.7% and 38.7%), and β-strand the least populated (8.4% and 4.3%). Upon addition of EGCG, the turn and α-helix are marginally enhanced (14.7 versus 18.0%, and 11.1 versus 13.4%) and the bend is slightly reduced (29% versus 25.6%). While the averaged propensities over all amino acids are rather

dx.doi.org/10.1021/jp312573y | J. Phys. Chem. B 2013, 117, 3993−4002

Table 1. Averaged Secondary Structure Propensities for the Aβ2 and Aβ2−EGCG Systems

secondary structures	coil (%)	bend (%)	turn (%)	β (%)	helix (%)
Aβ2	36.7 (0.2[a])	29.0 (0.1)	14.7 (0.06)	8.4[b] (0.01)	11.1 (0.01)
Aβ2−EGCG	38.7 (0.04)	25.6 (0.02)	18.0 (0.07)	4.3 (0.009)	13.4 (0.05)

[a]The numbers in parentheses are statistical errors estimated by Bootstrap analysis. [b]Note that the β-strand content varies from 8.2 to 8.4% for Aβ2 and from 4.1 to 4.3% for Aβ2−EGCG by using 100−180 ns and 100−200 ns time intervals, respectively.

similar in both systems, the per residue propensities differ for coil, β-strand, and α-helix. Upon EGCG interaction, the coil character of the N-terminal and loop regions is enhanced as shown in Figure 4. The β-strand propensity is very much reduced in the N-terminal region (varying from 10% to 1−2%), the CHC of chain 1 and the residues 39−42 (from 20% to 5%). In contrast, the β-strand content of the positions 30−38 is not impacted (Figure 7A). Finally, in the presence of EGCG, the

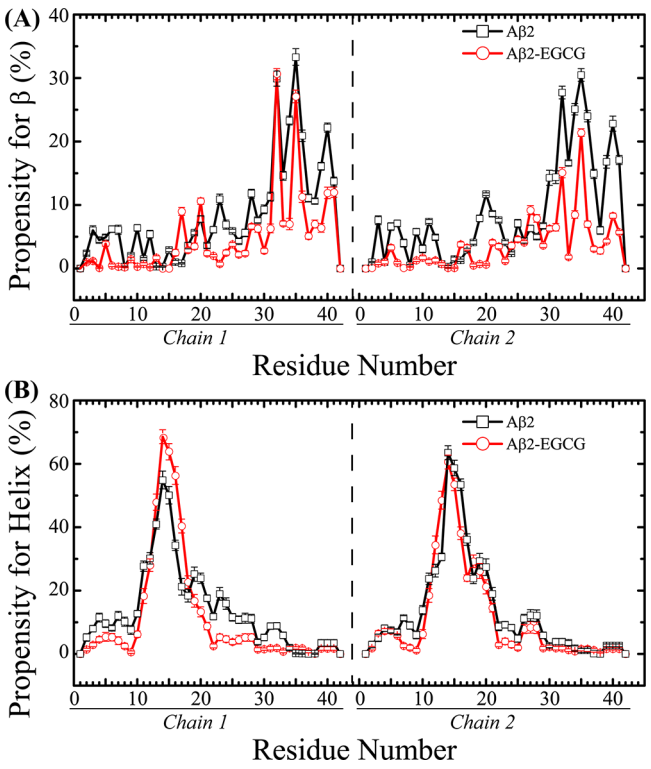

Figure 7. Secondary structure propensities as a function of each Aβ amino acid in both system at 315K. (A) The β-strand propensities along the amino acid sequence in Aβ2 (black line) and Aβ2−EGCG systems (red line). The vertical dashed line separates the two chains (B) same as A for α helix. Error bars are shown.

intensity of the α-helix peak centered at position His13 varies from 50 to 70% in chain 1(Figure 7B), and the intensity of the second peak at position His 14 in chain 2 remains mainly constant around 65%.

The free energy surfaces (FES) and the dominant structures from dihedral PCA analysis are shown in Figure 8. The free energy landscape of Aβ2−EGCG is broader and more complex than that of Aβ2, consistent with the fact that Aβ dimer without EGCG has higher conformational entropy (Figure 2B). The three and four most populated structures (with free energies <0.3 kcal/mol) of Aβ2 and Aβ2−EGCG, respectively, with their collision cross sections (CCS) are also shown. The most populated minimum (22%) in Aβ2, A1 (Figure 8A), with a CCS of 1243 Å^2, is essentially random coil, albeit three helices spanning either the CHC or the flanking CHC amino acids are formed. The two other less populated Aβ2 minima have a CCS of 1275 Å^2 (A2) and 1210 Å^2 (A3). The A2 configuration displays an intermolecular antiparallel β-sheet spanning 32−36 and 33−37, and a α-helix spanning 13−18 in one chain, while the A3 minimum is very disordered with only one α-helix spanning residues 3−8. The presence of EGCG molecules significantly increases the CCS values of Aβ and leads to different conformations (Figure 8B): the most populated B1 state (13%) has a CCS of 1363 Å^2, and the three other less populated states are characterized by B2 (1458 Å^2), B3 (1469 Å^2), and B4 (1432 Å^2). The B1 configuration displays two α-helices spanning 10−16 in one chain, and 13−17 in the other chain. The dimeric interface is free of any secondary structures and is characterized by interactions between the two N-terminals in an antiparallel-like orientation and between CHC and the fibril-loop region in a parallel-like orientation. The B2 configuration is almost fully coil/turn in character, except a short α-helix spanning 14−17 in one chain, and is characterized by N-terminal to N-terminal interactions in an antiparallel-like orientation. The B3 minimum displays a helix spanning 14−21 in one chain, while the second chain is random coil. Different from B1, B2m and B4, the two peptides in B3 are not directly interacting with each other, but mediated by EGCG. Finally, the B4 configuration displays two helices spanning 13−17 in one chain and 11−17 in the other chain. The interface is free of any secondary structures and composed of the fibril-loop region and the C-terminal in antiparallel orientation. Note that the error bar for the CCS is 1.2% if we use 10 structures rather than one single conformation around each minimum for both systems.

3.4. Effects of EGCG on the Interchain and Intrachain Interactions of Aβ Dimer. Figure 3B gives the total interchain contact numbers between the Aβ peptides for both systems. We see decreased interchain interactions in the Aβ2−EGCG system. Notably, 5.2(±0.3)% of the total configurations in the Aβ2−EGCG system consist of two separated monomers (number of interchain contacts = 0). In detail, the interchain interactions were further assessed by the side-chain−side-chain probability contact maps (Figure 9). For the Aβ2 system, the interpeptide interface mainly involves the CHC and the C-terminal region, as the regions of highest contact probability are C-terminal/C-terminal, CHC/CHC and CHC/C-terminal (Figure 9A). For the Aβ2−EGCG system, the interchain hydrophobic interactions are weakened in that the C-terminal/C-terminal and CHC/CHC interaction pairs almost disappear, while the C-terminal/CHC pair remains, but with a smaller probability (Figure 9B). We also note that the salt bridge propensities of the positively charged Arg5, K16, and K28 residues with the negatively charges residues D1, E3, D7, E11, E22, and D23 are small in both systems and are even lowered in the Aβ2−EGCG system (Supporting Information, Table S1). The intrachain side-chain−side-chain probability contact maps are shown in Figure S3 in the Supporting Information. We see that the CHC/C-terminal interaction is very much reduced

dx.doi.org/10.1021/jp312573y | J. Phys. Chem. B 2013, 117, 3993−4002

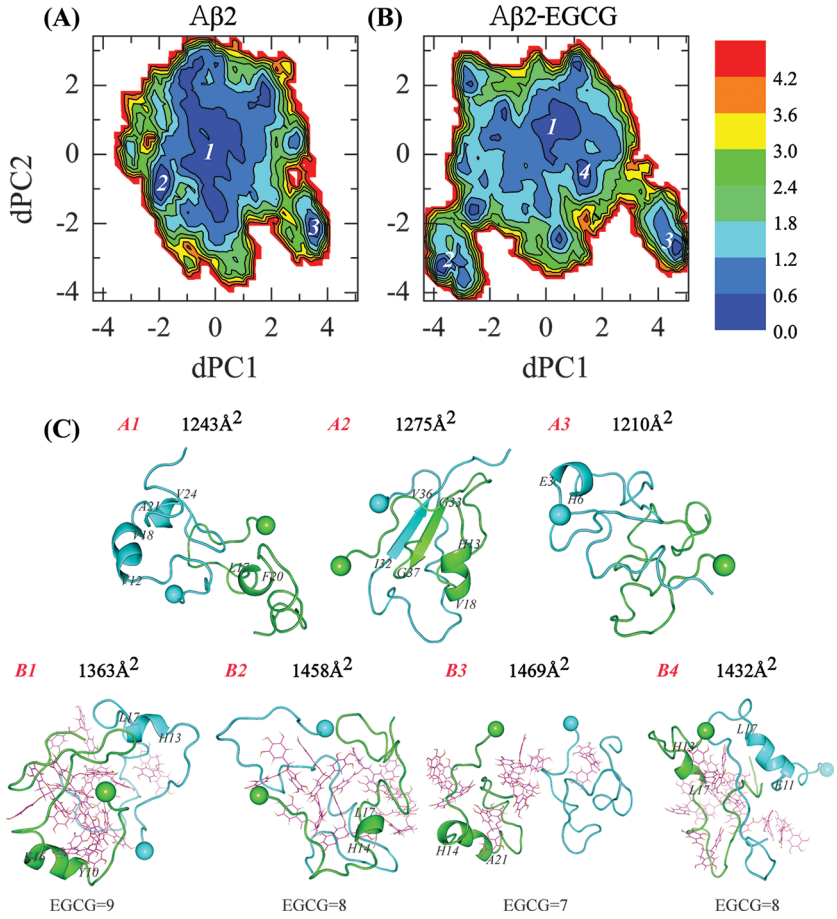

Figure 8. Free energy landscapes (in kcal/mol) and representative structures of the minima with free energy lower than 0.3 kcal/mol. The two Aβ chains are colored in green and cyan, and the EGCG molecules in magenta. The balls refer to the Cα atoms of the N-terminal residues D1. The numbers in Å^2 are the computed collision cross sections. (A) Aβ2 system, representative structures of the three dominant minima (A1, A2, and A3). (B) Aβ2−EGCG system, representative structures of the four dominant minima (B1, B2, B3, and B4).

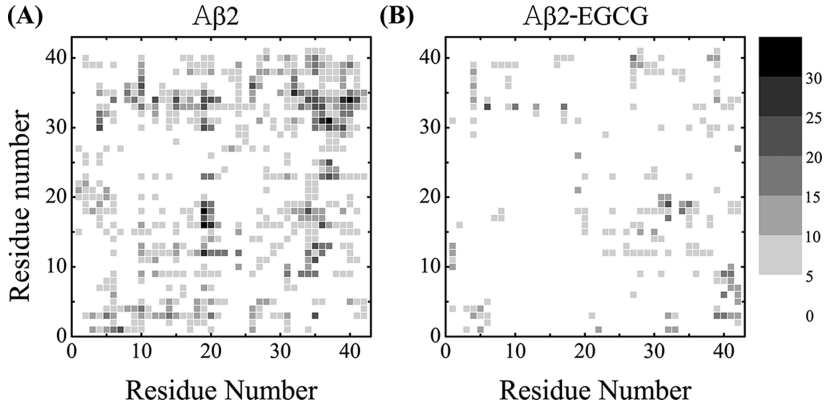

Figure 9. Intermolecular side-chain−side-chain contact maps. The color scale refers to the contact probability in the Aβ2 system (A) and in the Aβ2−EGCG system (B). To clarify, the same color scale is used for both systems.

upon addition of EGCG. Looking at all possible salt bridges, all long-range interactions have propensities <20% and are rather unaffected by EGCG, except the E22−K28 salt bridge decreasing from 16.6% to 6.8% (Supporting Information, Table S1). Finally, the averaged numbers of intra- and intermolecular H-bonds in the dimer do not change much, except a variation of 3% for the intermolecular main-chain H-bonds in the presence of EGCG (Supporting Information, Table S2).

3.5. Effects of EGCG on the Binding Energy of Aβ Dimer. The binding free energies, and their various contribution terms, are listed in Table 2 for the Aβ dimer in solution, and the Aβ2−EGCG complex. It is found that the Aβ dimer−EGCG complex is much more stable than the dimer in solution, $\Delta G_{binding}$ of −136.1 versus −91.2 kcal/mol. The molecular mechanics energy (ΔE_{GAS}) is the sum of ΔE_{ELE} and ΔE_{VDW}, and the solvation free energy (ΔG_{SOL}) is the sum of ΔG_{PS} and ΔG_{NPS}. From Table 2, it is found that both ΔE_{GAS}

dx.doi.org/10.1021/jp312573y | J. Phys. Chem. B 2013, 117, 3993−4002

Table 2. Binding Free Energy Decomposition of the Aβ2 and Aβ2−EGCG Systems Given by the MM/PBSA Method

energy[a] (kcal/mol)	Aβ2 Aβ dimer[b]	Aβ2−EGCG Aβ dimer−EGCG complex[c]
ΔE_{ELE}	−23.44 (3.03[d])	−254.53 (4.64)
ΔE_{VDW}	−111.76 (1.33)	−222.31 (1.61)
ΔE_{GAS}	−135.19 (3.86)	−476.82 (3.03)
ΔG_{NPS}	−12.77 (0.14)	−28.36 (0.18)
ΔG_{PS}	56.74 (3.03)	369.09 (4.05)
ΔG_{SOL}	43.96 (2.93)	340.73 (3.87)
$\Delta G_{binding}$	−91.24 (1.20)	−136.09 (0.85)

[a] $\Delta E_{GAS} = \Delta E_{ELE} + \Delta E_{VDW}$; $\Delta G_{SOL} = \Delta G_{NPS} + \Delta G_{PS}$; $\Delta G_{binding} = \Delta E_{GAS} + \Delta G_{SOL}$. [b] The binding free energy for the Aβ dimer is given by eq 3 in the Supporting Information. [c] The binding free energy for the Aβ dimer−EGCG complex is given by eq 4 in the Supporting Information. [d] The numbers in parentheses are the statistical errors estimated by Bootstrap analysis.

(−476.82 kcal/mol) and ΔG_{NPS} (−28.3 kcal/mol) are favorable for the formation of the Aβ dimer−EGCG complex, and ΔE_{ELE} and ΔE_{VDW} contribute to 50% and 44%. In contrast, the polar solvation energy (ΔG_{PS}) behaves oppositely (369 kcal/mol). This contribution of each term is consistent with MD simulations of $A\beta_{1-42}$ monomer with EGCG.[26]

4. DISCUSSION

Thus far, there are no available experimental structures of the $A\beta_{1-42}$ dimer in aqueous solution.[10] Bernstein et al. were, however, able to determine a collision cross-section area of 1256 Å^2 for $A\beta_{1-42}$ dimer using ion-mobility spectrometry.[9] Our calculated collision cross sections of 1243, 1275, and 1210 Å^2 for the three most populated states by dihedral PCA analysis nicely fit to their experiments.

Our analysis of secondary structure indicates that the $A\beta_{1-42}$ dimer mostly populates coil/turn (80.4%), and then α-helix and β-strand with 11.1% and 8.4%. The latter values do not match exactly but are consistent with the CD-derived values: a α-helix content varying from 3% to 9% and a β-strand content varying between 12% and 25%. It has to be noted, however, that the CD analysis at day 0 was performed, however, on a mixture of monomers and various aggregates.[10,11] Our results can be compared to the other simulations on $A\beta_{1-42}$ dimer. Using 50 ns all-atom MD simulations, Barz and Urbanc found a β-strand propensity of 6.6% of and a α-helix of 1% using the SPCE water model.[17] Using DMD simulations, the β-strand and α-helix contents were estimated to be 20% and 0.1%.[63] Other simulations using implicit solvent coupled with either a coarse-grained model[13] or an all-atom model[14] lead to a β-strand propensity of 25% and a α-helix propensity of <5% . Looking at the per residue propensity for β-strand, our simulations show that the C-terminal region is the most β-rich region. This is consistent with all previous simulations using either all-atom or coarse-grained models on $A\beta_{1-42}$ dimer.[13,14,17,28]

Looking at the networks of interchain contacts, our results show that the interface of the $A\beta_{1-42}$ dimer is mainly composed of the C-terminal and CHC regions. This is in agreement with many previous simulations, although the generated morphologies obtained are very different. These simulations include coarse-grained approach for $A\beta_{1-42}$ dimer[13,17] and $A\beta_{17-42}$ trimer,[33] an all-atom MC simulation with implicit solvent on $A\beta_{1-42}$ dimer,[14] and the more recent all-atom MD simulation coupled with SPCE or TIP3P solvent.[17]

Experimentally, EGCG has been reported to redirect the aggregation of the $A\beta_{1-42}$ peptide[22] into unstructured, off-pathway oligomers. In contrast to this experimental study, Reif et al. recently determined by solution-state NMR that the residues 29−36 in the EGCG-induced Aβ oligomers adopt a β-sheet configuration, whereas the residues 1−20 are unstructured. Our simulations cannot elucidate this structural variation since the oligomer and even monomer properties differ from $A\beta_{1-40}$ to $A\beta_{1-42}$.[11,13,27,63−65] In our equilibrium structures, we do not find any evidence of a well-formed β-sheet configuration, but rather find that the first 11 residues are essentially disordered and the residues 12−17 have a non-negligible probability for α-helix. It has to be noted also that our pattern of interactions between EGCG and $A\beta_{1-42}$ is fully consistent with that derived from isothermal titration calorimetry experiments[24,25] and not so different from that deduced from all-atom MD simulations of $A\beta_{1-42}$ monomer with EGCG molecules.[26]

5. CONCLUSION

To the best of our knowledge, this is the first extensive replica-exchange molecular dynamics study on $A\beta_{1-42}$ dimer with all-atom model and explicit solvent in the presence and absence of EGCG molecules. Though different force fields may generate different free energy landscapes,[37,66] our results on the pure $A\beta_{1-42}$ dimer based on the OPLS force field are in fair agreement with the experimental collision cross section and isothermal titration calorimetry data. The beta-rich character of the C-terminal region is also consistent with previous simulations using different force fields, albeit our morphologies of $A\beta_{1-42}$ dimer are very different. This indicates that OPLS-AA force field coupled to the SPC model is suitable for the dimerization of $A\beta_{1-42}$. Our REMD simulations on the $A\beta_{1-42}$ dimer−EGCG complex disclose that the binding of EGCG causes remarkable changes in the Aβ dimer, in terms of secondary structures, interchain interactions, morphologies, and binding free-energy profiles. Although the binding of EGCG reduces the β-content of Aβ dimer by 4(±1)% only, the reduction is significant in the C-terminal region resulting in a less-fibril state, and also to a lesser extent in the N-terminal region. We also find that, in the presence of EGCG, the CHC/CHC and C-terminal/C-terminal interactions observed in pure Aβ dimer are greatly reduced, resulting in an increase of 8(±1.2)% of the collision cross sections of Aβ dimer, and a population of 5.2(±0.3)% of two separated monomers. Overall, our all-atom simulations in explicit solvent provide for the first time insights on the $A\beta_{1-42}$ dimeric structures and an atomic picture of the EGCG-mediated conformational change on $A\beta_{1-42}$ dimer, thereby contributing to a better understanding of the molecular mechanism of inhibition of EGCG on the $A\beta_{1-42}$ dimer.

It has to be emphasized that, despite the present simulations being carried out in neat water at pH 7 and 315 K, the main results should not vary much at physiological conditions (pH 7.4, 310 K and 100 mmol/L NaCl) even if the binding of EGCG to $A\beta_{1-42}$ and the hydrophobic interactions are slightly promoted, and the hydrogen-bonding interactions are less favored by increasing salt concentration.[24]

dx.doi.org/10.1021/jp312573y | J. Phys. Chem. B 2013, 117, 3993−4002

■ ASSOCIATED CONTENT

Supporting Information

The distribution of fraction of buried surface area (BSA) for EGCG molecules. The occupancy of hydrogen bonds between Aβ amino acids and EGCG. The intrachain heavy atom contact maps for Aβ peptides. Salt-bridge propensity. Hydrogen bonds in the Aβ2 and Aβ2−EGCG systems. The derived force field parameters for EGCG molecule. Complete author list for refs 9, 18, 20, 31, 39, 40, 58, and 59. This material is available free of charge via the Internet at http://pubs.acs.org.

■ AUTHOR INFORMATION

Corresponding Author

*Phone: (65)63162885. E-mail: ygmu@ntu.edu.sg

Notes

The authors declare no competing financial interest.

■ ACKNOWLEDGMENTS

The authors gratefully thank the support of the French-Singapore MERLION Ph.D. 2010 program (project 5.08.10). This work was partially supported by the IDA Cloud Computing Call 4, NTU Tier 1 grant RG 23/11 and the A*STAR Computational Resource Centre (http://www.acrc.a-star.edu.sg) through the use of its high performance computing facilities.

■ REFERENCES

(1) Selkoe, D. J. Folding proteins in fatal ways. *Nature* **2003**, *426* (6968), 900−904.

(2) Dobson, C. M. Protein folding and misfolding. *Nature* **2003**, *426* (6968), 884−890.

(3) Taylor, J. P.; Hardy, J.; Fischbeck, K. H. Biomedicine - Toxic proteins in neurodegenerative disease. *Science* **2002**, *296* (5575), 1991−1995.

(4) Sacchettini, J. C.; Kelly, J. W. Therapeutic strategies for human amyloid diseases. *Nat. Rev. Drug Discov.* **2002**, *1* (4), 267−275.

(5) Walsh, D. M.; Klyubin, I.; Fadeeva, J. V.; Cullen, W. K.; Anwyl, R.; Wolfe, M. S.; Rowan, M. J.; Selkoe, D. J. Naturally secreted oligomers of amyloid [beta] protein potently inhibit hippocampal long-term potentiation in vivo. *Nature* **2002**, *416* (6880), 535−539.

(6) Thompson, L. K. Unraveling the secrets of Alzheimer's β-amyloid fibrils. *Proc. Natl. Acad. Sci. U.S.A.* **2003**, *100* (2), 383−385.

(7) Kirkitadze, M. D.; Bitan, G.; Teplow, D. B. Paradigm shifts in Alzheimer's disease and other neuro degenerative disorders: The emerging role of oligomeric assemblies. *J. Neurosci. Res.* **2002**, *69* (5), 567−577.

(8) Klein, W. L.; Stine, W. B.; Teplow, D. B. Small assemblies of unmodified amyloid beta-protein are the proximate neurotoxin in Alzheimer's disease. *Neurobiol. Aging* **2004**, *25* (5), 569−580.

(9) Bernstein, S. L.; Dupuis, N. F.; Lazo, N. D.; Wyttenbach, T.; Condron, M. M.; Bitan, G.; Teplow, D. B.; Shea, J.-E.; Ruotolo, B. T.; Robinson, C. V.; et al. Amyloid-β protein oligomerization and the importance of tetramers and dodecamers in the aetiology of Alzheimer's disease. *Nat. Chem.* **2009**, *1* (4), 326−331.

(10) Kirkitadze, M. D.; Condron, M. M.; Teplow, D. B. Identification and characterization of key kinetic intermediates in amyloid β-protein fibrillogenesis. *J. Mol. Biol.* **2001**, *312* (5), 1103−1119.

(11) Ono, K.; Condron, M. M.; Teplow, D. B. Structure−neurotoxicity relationships of amyloid β-protein oligomers. *Proc. Natl. Acad. Sci. U.S.A.* **2009**, *106* (35), 14745−14750.

(12) Urbanc, B.; Cruz, L.; Ding, F.; Sammond, D.; Khare, S.; Buldyrev, S. V.; Stanley, H. E.; Dokholyan, N. V. Molecular Dynamics Simulation of Amyloid 2 Dimer Formation. *Biophys. J.* **2004**, *87* (4), 2310−2321.

(13) Côté, S.; Laghaei, R.; Derreumaux, P.; Mousseau, N. Distinct Dimerization for Various Alloforms of the Amyloid-Beta Protein: Aβ1−40, Aβ1−42, and Aβ1−40(D23N). *J. Phys. Chem. B* **2012**, *116*, 4043−4055.

(14) Mitternacht, S.; Staneva, I.; Härd, T.; Irbäck, A. Monte Carlo Study of the Formation and Conformational Properties of Dimers of Aβ42 Variants. *J. Mol. Biol.* **2011**, *410* (2), 357−367.

(15) Chong, S.-H.; Ham, S. Atomic-level investigations on the amyloid-[small beta] dimerization process and its driving forces in water. *Phys. Chem. Chem. Phys.* **2012**, *14* (5), 1573−1575.

(16) Zhu, X.; Bora, R. P.; Barman, A.; Singh, R.; Prabhakar, R. Dimerization of the Full-Length Alzheimer Amyloid β-Peptide (Aβ42) in Explicit Aqueous Solution: A Molecular Dynamics Study. *J. Phys. Chem. B* **2012**, *116*, 4405−4416.

(17) Barz, B.; Urbanc, B. Dimer Formation Enhances Structural Differences between Amyloid β-Protein (1−40) and (1−42): An Explicit-Solvent Molecular Dynamics Study. *PLoS ONE* **2012**, *7* (4), e34345.

(18) Frydman-Marom, A.; Levin, A.; Farfara, D.; Benromano, T.; Scherzer-Attali, R.; Peled, S.; Vassar, R.; Segal, D.; Gazit, E.; Frenkel, D.; et al. Orally Administrated Cinnamon Extract Reduces β-Amyloid Oligomerization and Corrects Cognitive Impairment in Alzheimer's Disease Animal Models. *PLoS ONE* **2011**, *6* (1), e16564.

(19) Chen, J.; Armstrong, A. H.; Koehler, A. N.; Hecht, M. H. Small Molecule Microarrays Enable the Discovery of Compounds That Bind the Alzheimer's Aβ Peptide and Reduce its Cytotoxicity. *J. Am. Chem. Soc.* **2010**, *132*, 17015−17022.

(20) Scherzer-Attali, R.; Pellarin, R.; Convertino, M.; Frydman-Marom, A.; Egoz-Matia, N.; Peled, S.; Levy-Sakin, M.; Shalev, D. E.; Caflisch, A.; Gazit, E.; et al. Complete Phenotypic Recovery of an Alzheimer's Disease Model by a Quinone-Tryptophan Hybrid Aggregation Inhibitor. *PLoS ONE* **2010**, *5* (6), e11101.

(21) Mishra, R.; Sellin, D.; Radovan, D.; Gohlke, A.; Winter, R. Inhibiting Islet Amyloid Polypeptide Fibril Formation by the Red Wine Compound Resveratrol. *ChemBioChem* **2009**, *10* (3), 445−449.

(22) Ehrnhoefer, D. E.; Bieschke, J.; Boeddrich, A.; Herbst, M.; Masino, L.; Lurz, R.; Engemann, S.; Pastore, A.; Wanker, E. E. EGCG redirects amyloidogenic polypeptides into unstructured, off-pathway oligomers. *Nat. Struct. Mol. Biol.* **2008**, *15* (6), 558−566.

(23) Bieschke, J.; Russ, J.; Friedrich, R. P.; Ehrnhoefer, D. E.; Wobst, H.; Neugebauer, K.; Wanker, E. E. EGCG remodels mature alpha-synuclein and amyloid-beta fibrils and reduces cellular toxicity. *Proc. Natl. Acad. Sci. U.S.A.* **2010**, *107* (17), 7710−7715.

(24) Wang, S.-H.; Liu, F.-F.; Dong, X.-Y.; Sun, Y. Thermodynamic Analysis of the Molecular Interactions between Amyloid β-Peptide 42 and (−)-Epigallocatechin-3-gallate. *J. Phys. Chem. B* **2010**, *114*, 11576−11583.

(25) Wang, S.-H.; Dong, X.-Y.; Sun, Y. Thermodynamic Analysis of the Molecular Interactions between Amyloid β-Protein Fragments and (−)-Epigallocatechin-3-gallate. *J. Phys. Chem. B* **2012**, *116*, 5803−5809.

(26) Liu, F.-F.; Dong, X.-Y.; He, L.; Middelberg, A. P. J.; Sun, Y. Molecular Insight into Conformational Transition of Amyloid β-Peptide 42 Inhibited by (−)-Epigallocatechin-3-gallate Probed by Molecular Simulations. *J. Phys. Chem. B* **2011**, *115*, 11879−11887.

(27) Côté, S. b.; Derreumaux, P.; Mousseau, N. Distinct Morphologies for Amyloid Beta Protein Monomer: Aβ1−40, Aβ1−42, and Aβ1−40(D23N). *J. Chem. Theory Comput.* **2011**, *7* (8), 2584−2592.

(28) Melquiond, A.; Dong, X.; Mousseau, N.; Derreumaux, P. Role of the Region 23−28 in A Fibril Formation: Insights from Simulations of the Monomers and Dimers of Alzheimers Peptides A40 and A42. *Curr. Alzheimer Res.* **2008**, *5* (3), 244−250.

(29) Wu, C.; Scott, J.; Shea, J.-E. Binding of Congo Red to Amyloid Protofibrils of the Alzheimer Aβ9−40 Peptide Probed by Molecular Dynamics Simulations. *Biophys. J.* **2012**, *103* (3), 550−557.

(30) Zhao, L. N.; Chiu, S.-W.; Benoit, J.; Chew, L. Y.; Mu, Y. The Effect of Curcumin on the Stability of Aβ Dimers. *J. Phys. Chem. B* **2012**, *116*, 7428−7435.

(31) Sinha, S.; Lopes, D. H. J.; Du, Z.; Pang, E. S.; Shanmugam, A.; Lomakin, A.; Talbiersky, P.; Tennstaedt, A.; McDaniel, K.; Bakshi, R.;

et al. Lysine-Specific Molecular Tweezers Are Broad-Spectrum Inhibitors of Assembly and Toxicity of Amyloid Proteins. *J. Am. Chem. Soc.* **2011**, *133*, 16958−16969.
(32) Takeda, T.; Chang, W. E.; Raman, E. P.; Klimov, D. K. Binding of nonsteroidal anti-inflammatory drugs to Aβ fibril. *Proteins: Struct., Funct., Bioinf.* **2010**, *78* (13), 2849−2860.
(33) Chebaro, Y.; Jiang, P.; Zang, T.; Mu, Y.; Nguyen, P. H.; Mousseau, N.; Derreumaux, P. Structures of Aβ17−42 Trimers in Isolation and with Five Small-Molecule Drugs Using a Hierarchical Computational Procedure. *J. Phys. Chem. B* **2012**, *116*, 8412−8422.
(34) Crescenzi, O.; Tomaselli, S.; Guerrini, R.; Salvadori, S.; D'Ursi, A. M.; Temussi, P. A.; Picone, D. Solution structure of the Alzheimer amyloid β-peptide (1−42) in an apolar microenvironment. *Eur. J. Biochem.* **2002**, *269* (22), 5642−5648.
(35) Jorgensen, W. L.; Tirado-Rives, J. The OPLS [optimized potentials for liquid simulations] potential functions for proteins, energy minimizations for crystals of cyclic peptides and crambin. *J. Am. Chem. Soc.* **1988**, *110*, 1657−1666.
(36) Sgourakis, N. G.; Yan, Y.; McCallum, S. A.; Wang, C.; Garcia, A. E. The Alzheimer's Peptides Aβ40 and 42 Adopt Distinct Conformations in Water: A Combined MD/NMR Study. *J. Mol. Biol.* **2007**, *368* (5), 1448−1457.
(37) Nguyen, P. H.; Li, M. S.; Derreumaux, P. Effects of all-atom force fields on amyloid oligomerization: replica exchange molecular dynamics simulations of the A[small beta]16−22 dimer and trimer. *Phys. Chem. Chem. Phys.* **2011**, *13* (20), 9778−9788.
(38) Reddy, G.; Straub, J. E.; Thirumalai, D. Influence of Preformed Asp23−Lys28 Salt Bridge on the Conformational Fluctuations of Monomers and Dimers of Aβ Peptides with Implications for Rates of Fibril Formation. *J. Phys. Chem. B* **2009**, *113*, 1162−1172.
(39) Shao, Y.; Molnar, L. F.; Jung, Y.; Kussmann, J.; Ochsenfeld, C.; Brown, S. T.; Gilbert, A. T. B.; Slipchenko, L. V.; Levchenko, S. V.; O'Neill, D. P.; et al. Advances in methods and algorithms in a modern quantum chemistry program package. *Phys. Chem. Chem. Phys.* **2006**, *8* (27), 3172−3191.
(40) Frisch, M. J.; Trucks, G. W.; Schlegel, H. B.; Scuseria, G. E.; Robb, M. A.; Cheeseman, J. R.; Scalmani, G.; Barone, V.; Mennucci, B.; Petersson, G. A.; et al. *Gaussian 09, Revision B.01*; Gaussian Inc.: Wallingford, CT, 2009.
(41) Dupradeau, F. Y.; Pigache, A.; Zaffran, T.; Savineau, C.; Lelong, R.; Grivel, N.; Lelong, D.; Rosanski, W.; Cieplak, P. The R.ED. tools: advances in RESP and ESP charge derivation and force field library building. *Phys. Chem. Chem. Phys.* **2010**, *12* (28), 7821−7839.
(42) Hermans, J.; Berendsen, H. J. C.; Vangunsteren, W. F.; Postma, J. P. M. A Consistent Empirical Potential for Water-Protein Interactions. *Biopolymers* **1984**, *23* (8), 1513−1518.
(43) Hu, Z.; Jiang, J. Assessment of biomolecular force fields for molecular dynamics simulations in a protein crystal. *J. Comput. Chem.* **2010**, *31* (2), 371−380.
(44) Van der Spoel, D.; Lindahl, E.; Hess, B.; Groenhof, G.; Mark, A. E.; Berendsen, H. J. C. GROMACS: Fast, flexible, and free. *J. Comput. Chem.* **2005**, *26* (16), 1701−1718.
(45) Hess, B.; Bekker, H.; Berendsen, H. J. C.; Fraaije, J. LINCS: A linear constraint solver for molecular simulations. *J. Comput. Chem.* **1997**, *18* (12), 1463−1472.
(46) Essmann, U.; Perera, L.; Berkowitz, M. L.; Darden, T.; Lee, H.; Pedersen, L. G. A Smooth Particle Mesh Ewald Method. *J. Chem. Phys.* **1995**, *103* (19), 8577−8593.
(47) Hansmann, U. H. E. Parallel tempering algorithm for conformational studies of biological molecules. *Chem. Phys. Lett.* **1997**, *281* (1−3), 140−150.
(48) Sugita, Y.; Okamoto, Y. Replica-exchange molecular dynamics method for protein folding. *Chem. Phys. Lett.* **1999**, *314* (1−2), 141−151.
(49) Patriksson, A.; van der Spoel, D. A temperature predictor for parallel tempering simulations. *Phys. Chem. Chem. Phys.* **2008**, *10* (15), 2073−2077.
(50) Bussi, G.; Donadio, D.; Parrinello, M. Canonical sampling through velocity rescaling. *J. Chem. Phys.* **2007**, *126* (1), 014101−7.
(51) Lerbret, A.; Bordat, P.; Affouard, F.; Hédoux, A.; Guinet, Y.; Descamps, M. How Do Trehalose, Maltose, and Sucrose Influence Some Structural and Dynamical Properties of Lysozyme? Insight from Molecular Dynamics Simulations. *J. Phys. Chem. B* **2007**, *111*, 9410−9420.
(52) Kabsch, W.; Sander, C. Dictionary of protein secondary structure: Pattern recognition of hydrogen-bonded and geometrical features. *Biopolymers* **1983**, *22* (12), 2577−2637.
(53) Mu, Y.; Nguyen, P. H.; Stock, G. Energy landscape of a small peptide revealed by dihedral angle principal component analysis. *Proteins: Struct., Funct., Bioinf.* **2005**, *58* (1), 45−52.
(54) Shvartsburg, A. A.; Jarrold, M. F. An exact hard-spheres scattering model for the mobilities of polyatomic ions. *Chem. Phys. Lett.* **1996**, *261* (1−2), 86−91.
(55) Mesleh, M. F.; Hunter, J. M.; Shvartsburg, A. A.; Schatz, G. C.; Jarrold, M. F. Structural Information from Ion Mobility Measurements: Effects of the Long-Range Potential. *J. Phys. Chem.* **1996**, *100*, 16082−16086.
(56) Dear, G. J.; Munoz-Muriedas, J.; Beaumont, C.; Roberts, A.; Kirk, J.; Williams, J. P.; Campuzano, I. Sites of metabolic substitution: investigating metabolite structures utilising ion mobility and molecular modelling. *Rapid Commun. Mass Spectrom.* **2010**, *24* (21), 3157−3162.
(57) Schlitter, J. Estimation of absolute and relative entropies of macromolecules using the covariance matrix. *Chem. Phys. Lett.* **1993**, *215* (6), 617−621.
(58) Kollman, P. A.; Massova, I.; Reyes, C.; Kuhn, B.; Huo, S.; Chong, L.; Lee, M.; Lee, T.; Duan, Y.; Wang, W.; et al. Calculating Structures and Free Energies of Complex Molecules: Combining Molecular Mechanics and Continuum Models. *Acc. Chem. Res.* **2000**, *33*, 889−897.
(59) Case, D. A.; Darden, T. A.; Cheatham, T. E.; Simmerling, C. L.; Wang, J.; Duke, R. E.; Luo, R.; Crowley, M.; Walker, R. C.; Zhang, W.; et al. *Amber 10*; University of California: San Francisco, 2008.
(60) Hou, T. J.; Wang, J. M.; Li, Y. Y.; Wang, W. Assessing the Performance of the MM/PBSA and MM/GBSA Methods. 1. The Accuracy of Binding Free Energy Calculations Based on Molecular Dynamics Simulations. *J. Chem Inf. Model.* **2011**, *51* (1), 69−82.
(61) Sitkoff, D.; Sharp, K. A.; Honig, B. Correlating solvation free energies and surface tensions of hydrocarbon solutes. *Biophys. Chem.* **1994**, *51* (2−3), 397−409.
(62) Gorfe, A. A.; Jelesarov, I. Energetics of Sequence-Specific Protein−DNA Association: Computational Analysis of Integrase Tn916 Binding to Its Target DNA. *Biochemistry* **2003**, *42* (40), 11568−11576.
(63) Urbanc, B.; Betnel, M.; Cruz, L.; Bitan, G.; Teplow, D. B. Elucidation of Amyloid β-Protein Oligomerization Mechanisms: Discrete Molecular Dynamics Study. *J. Am. Chem. Soc.* **2010**, *132*, 4266−4280.
(64) Bitan, G.; Kirkitadze, M. D.; Lomakin, A.; Vollers, S. S.; Benedek, G. B.; Teplow, D. B. Amyloid β-protein (Aβ) assembly: Aβ40 and Aβ42 oligomerize through distinct pathways. *Proc. Natl. Acad. Sci. U.S.A.* **2003**, *100* (1), 330−335.
(65) Yang, M.; Teplow, D. B. Amyloid β-Protein Monomer Folding: Free-Energy Surfaces Reveal Alloform-Specific Differences. *J. Mol. Biol.* **2008**, *384* (2), 450−464.
(66) Cao, Z. X.; Liu, L.; Zhao, L. L.; Wang, J. H. Effects of Different Force Fields and Temperatures on the Structural Character of Abeta (12−28) Peptide in Aqueous Solution. *Int. J. Mol. Sci.* **2011**, *12* (11), 8259−8274.